

Original Article

Synergistic inhibition effect of orange peel extract and potassium iodide on corrosion of Q235 steel in hydrochloric acid solution

Xinhua Liu^{a,*}, Siyu Liu^{a,b,*}, Hongxia Zhang^a, Yuan Zhang^a, Baojing Luo^a, Ying Wang^a, Xiaoyan Xu^a, Jiarui Du^a, Boxi Yang^a, Linyan Gu^a, Xingdi Zhao^a, Hengyong Wei^c^aDepartment of Chemistry, Tangshan Normal University, Tangshan, China^bDepartment of College of Chemical Engineering, Northwest Minzu University, Lanzhou, Gansu, China^cDepartment of College of Material Science and Engineering, North China University of Science and Technology, Tangshan, Hebei, China

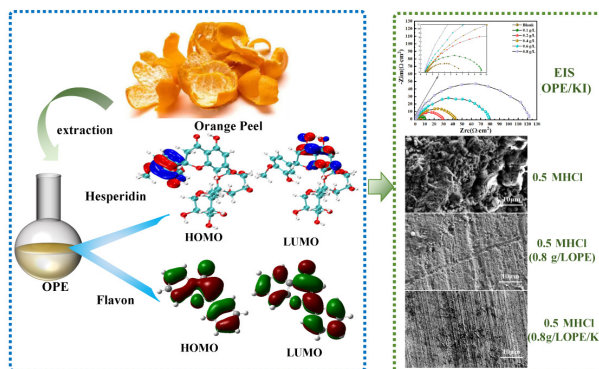
ARTICLE INFO

Keywords:

Corrosion inhibiting ability
Orange peel extract (OPE)
Q235 steel (QS)
Synergistic effect

ABSTRACT

Q235 steel (QS) is susceptible to corrosion. Organic compounds in orange peel, such as hesperidin and flavonoids, contain carbonyl, aromatic ring and hydroxyl functional groups. This enables them to interact with iron (Fe) to form a protective barrier and reduce QS corrosion in acidic solutions. In this study, we prepared a green and environmentally friendly anti-corrosion orange peel extract (OPE) using an anhydrous ethanol and acetone solution extraction method. We conducted a novel research on the synergistic corrosion-inhibiting impact of OPE and potassium iodide (KI) on QS in 0.50 M HCl. Theoretical calculations confirmed that hesperidin and flavonoid compounds of OPE could effectively reduce the corrosion of QS in acidic solutions. The weight loss method showed that OPE/KI demonstrated excellent corrosion inhibiting ability, reaching a rate of 97.05% corrosion inhibiting. In contrast, when used independently, OPE and KI showed corrosion inhibiting ability of corrosion inhibiting only 80.16% and 35.68%, respectively. Thus, it was confirmed that OPE and KI show a synergistic inhibition effect. Electrochemical tests proved the combined ability of OPE and KI as excellent corrosion inhibitors. Analyses of OPE/KI corrosion inhibitive mechanisms on QS were conducted utilizing scanning electron microscopy (SEM), Fourier transform infrared spectroscopy (FTIR), Contact angle (CA), atomic force microscopy (AFM), and X-ray photoelectron spectroscopy (XPS). The findings indicated that the OPE/KI created a protective barrier on the QS, which mitigated corrosion of QS in the acidic medium.



HOMO: Highest occupied molecular orbital, LUMO: Lowest unoccupied molecular orbital, PE: Orange peel extract

In this study, it has been proven by theoretical calculations that OPE has certain corrosion inhibiting abilities. Electrochemical experiments and weight-loss tests have demonstrated that the combination of OPE with KI exhibits excellent corrosion inhibiting ability. It promotes the efficient use of renewable resources.

*Corresponding authors:

E-mail addresses: hualiyiwang@163.com (X. Liu) liusiyu@aliyun.com (S. Liu)

Received: 29 October, 2024 Accepted: 31 December, 2024 Epub Ahead of Print: 10 March 2025 Published: 18 March 2025

DOI: 10.25259/AJC_120_2024

1. Introduction

Q235 steel (QS) is extensively utilized in the construction industry, manufacturing, and other fields for its cost-effectiveness, good plasticity, and high-tensile strength [1]. However, because of its high reactivity, QS is susceptible to corrosion, which not only leads to significant waste of metal materials but also causes serious economic losses globally [2]. Incorporating corrosion inhibitors into corrosive environments is a simple and efficient approach to slow down the corrosion damage to QS [3]. Plant extracts, for their cost-effectiveness, renewability, and environmental friendliness, find extensive application within the field of metallic material protection. In recent years, a substantial body of research has demonstrated that plant extracts could interact with metal surfaces to form a protective layer, reducing metal corrosion [4,5]. This is due to the protective film formed by the inhibitor effectively reducing direct contact between the corrosive medium and the metal, thereby serving to protect the metal [6-8]. To date, various parts of plants have been extensively studied, such as the *Veratrum* root [9], ginger [10], kapok leaf [11], coconut leaf [12], soybean [13], grape seed [14], and water celery [15]. Researchers have found that the anti-corrosive effect of botanical extracts are attributed to the rich content of sulfur, oxygen, nitrogen, conjugated heterocycles and polar groups. These enable the absorption of botanical extracts onto the metallic surface with high efficiency [16]. However, reliance on plant extracts alone as anti-corrosion agents has drawbacks such as unstable performance and low efficacy, which severely limits their application. To enhance the corrosion inhibiting ability of plant extracts, they are used in combination with other chemical compounds to leverage synergistic effects and effectively reduce the corrosion of metallic materials in acidic solutions.

The synergistic system composed of organic compounds and halogen ions (Cl, Br, I) demonstrates excellent corrosion inhibiting ability. Within these synergistic systems, the cooperative effect decreases as: I, Br, and Cl. This is because larger-sized halogen ions are more easily polarized due to their larger induced dipole moments. This helps the corrosion inhibitor be adsorbed onto the metallic surface and enhances their corrosion inhibiting ability. This demonstrates a synergistic corrosion inhibition effect between the halogen ions and the corrosion inhibitor [17]. Recently, the use of plant extracts mixed with halogen ions for their synergistic corrosion inhibition effect on metals in acidic environments has been a hot research topic. Li *et al.* [16] investigated the synergistic corrosion inhibition effect of walnut green husk extract (WGHE) and potassium iodide (KI) on cold rolled steel (CRS) in trichloroacetic acid (Cl_3CCOOH) solution. The results showed that the WGHE/KI mixture achieved a corrosion inhibition efficiency of up to 97.2%. Kaya *et al.* [18] showed that when 1000 ppm of KI was added to the acidic solution containing the *Rheum ribes* leaf extract, the corrosion inhibition efficiency increased from 91.8% to 94.9%. Bouhal *et al.* [19] studied the synergistic effect of coffee grounds extract (HECG) and KI on the protection of C38 steel in 1 M HCl medium. The results demonstrated that the inhibition efficiency reached 97%. This synergy was due to the presence of I, enhancing the stability of organic compounds' absorption. Thus, the combined use of plant extracts with KI shows promising results as a new type of highly effective green corrosion inhibitor.

Orange fruits are sweet and sour, rich in vitamins, phenols, flavonoids, minerals, and other nutrients, and are favored by consumers. They are one of the predominant raw materials utilized in the global juice marketplace and have always ranked first in terms of global juice consumption. While preparing orange juice, a large amount of orange peel is produced. A small amount of orange peel is currently used as the traditional Chinese medicine called "Chenpi," but most of it is discarded, causing significant waste generation and environmental pollution. Therefore, the utilization of orange peels is important. Hesperidin and flavonoids are the primary constituents of orange peel. These main components have the capacity to inhibit corrosion of metallic materials. For example, it had been reported in literature that OPE had a corrosion inhibiting effect on metals such as aluminum [20] and stainless steel [21] in corrosive environments. However, the corrosion inhibiting ability of OPE needs to be enhanced. Given the

complexity of substances in plant extracts, further exploration is needed to understand the synergistic mechanisms between plant extracts and halogen ions. Therefore, in this study, I and OPE were used to explore the synergistic corrosion inhibition mechanisms of I and OPE as inhibitors. The influence of I on the corrosion inhibiting properties of OPE in acidic media was also examined in this experiment. Therefore, in this study, taking I and OPE as examples, the synergistic corrosion inhibition mechanism of I and OPE were investigated for the first time. Further insights into the synergistic inhibition mechanism between plant extracts and iodide ions were gained. At the same time, this research promotes the efficient use of OPE as a corrosion inhibitor in the field of metal protection.

This investigation was based on the concept of cost-effective and environmentally friendly corrosion protection, utilizing OPE in conjunction with KI as a corroding inhibitor. The study probed the inhibitory effects of a blend of OPE and KI on QS corrosion in 0.5 M HCl. During the pickling process, to avoid the generation of HCl acid fog, the environmental temperature should not be too high. To be cost-effective, the consumption of acid should also be minimized. For these reasons, the HCl concentration was 0.5 M in this study. Fourier transform infrared spectroscopy (FTIR) and UV-vis spectroscopy were used to analyze the presence of hesperidin and flavonoids, the two main compounds in OPE. The inhibited corrosion mechanics of OPE were studied through theoretical calculations. Furthermore, the weight loss method and electrochemical experiments were employed to explore the corrosion inhibiting capacity of OPE/KI. The micromorphology and composition of the QS surface were characterized utilizing scanning electron microscope (SEM), Fourier transform infrared spectroscopy (FTIR), contact angle (CA), X-ray photoelectron spectroscopy (XPS), and atomic force microscopy (AFM). The results indicated that the synergistic effect of I and OPE could effectively reduce the corrosion of QS in hydrochloric acid solution.

2. Materials and Methods

2.1. Materials

The main components of QS are: C (0.45%), Mn (0.5%), Si (0.18%), P (0.035%), S (0.035%), Cr (0.25%), Ni (0.30%), Cu (0.25%), and Fe (the remaining 98%). In this experiment, the weight loss method employed standard Type II carbon steel plates, characterized by a 20 cm² area and a density of 7.86 g/cm³. The QS surface was first cleaned with a degreasing cotton pad, then rinsed with distilled water, degreased with acetone, and dried in cooled air. Dilute 37% AR-grade HCl with distilled water to make a 0.5 M HCl.

2.2. Extraction of OPE

Orange peels were sourced from Jiangxi, China. The dried orange peels were ground into a powdered substance. The powder was combined with anhydrous ethanol and acetone in a 1:10:10 ratio. Then they were placed in a water bath at 50°C to 60°C for 2 hrs. The extract was filtered, and filtrate was evaporated and dried in a well-ventilated oven for future application.

2.3. Characterization of OPE

The structure of the OPE was characterized by using a VERTEX70 FTIR and a UV-2550 Ultraviolet-Visible Spectrophotometer (UV-vis).

2.4. Weightlessness measurement method

According to the reference [22], the treated QS samples were accurately weighed and soaked in 0.5 M HCl solutions that contained varying contents of OPE, KI or OPE/KI for 6 hrs. The corroded QS was washed with distilled water and anhydrous ethanol, then dried and its weight was recorded again. The corrosion rate (v) was estimated using Eq. (1), which considers the weight loss of QS (w), its surface area (s), and the exposure time (t) to corrosion. The corrosion inhibiting efficiency (η_w) was derived from Eq. (2).

$$v = \frac{w}{s \times t} \quad (1)$$

$$\eta_w = \frac{v_0 - v}{v} \times 100\% \quad (2)$$

In the formulas, v_0 and v represented the corrosion rates of the QS sample in 0.5 M HCl with and without the inhibitor, respectively.

2.5. Electrochemical measurement

According to the reference [22], a saturated calomel electrode (SCE), platinum electrode were utilized as reference and counter electrodes, respectively. QS rods with an exposed 1 cm² area were utilized as working electrodes (WE). The experiment was conducted after the stabilization of open circuit potential (OCP). The Electrochemical Impedance Spectroscopy (EIS) tested from 0.01 to 10⁵ Hz, using a 10 mV AC signal. Polarization Curve (PDP) tests ranged from ±250 mV at a scanning velocity of 0.5 mV·s⁻¹. Data from EIS and PDP were analyzed with Zahner software. The corrosion inhibiting efficiency ($\eta\%$) of PDP measurements were determined by Eq. (3). The corrosion inhibiting efficiency ($\eta\%$) for the Electrochemical impedance spectroscopy (EIS) text was obtained through Eq. (4).

$$\eta(\%) = \frac{i_{cor}^0 - i_{cor}}{i_{cor}^0} \times 100\% \quad (3)$$

$$\eta(\%) = \frac{R_{ct} - R_{ct}^0}{R_{ct}} \times 100\% \quad (4)$$

In the formula, i_{cor} and i_{cor}^0 represented the corrosion current densities of hydrochloric acid solutions with and without OPE/KI, respectively. R_{ct} was the charge transfer resistance when OPE/KI was added, and R_{ct}^0 was the charge transfer resistance in the absence of OPE/KI.

2.6. Quantum chemical calculations

The research investigated the mechanisms by which hesperidin and flavonoids inhibit corrosion. Based on the B3LYP/Becke theory, the optimized geometric structures of hesperidin and flavonoid molecules were obtained using the Gaussian View software. The energy of the highest occupied molecular orbital (E_{HOMO}) and the lowest unoccupied molecular orbital (E_{LUMO}) of the main components; hesperidin and flavonoid in OPE were computed. The energy gaps (ΔE) were also obtained to evaluate their corrosion inhibiting ability. The number of electrons transferred (ΔN) between OPE and iron atoms could be calculated using the Pearson Eq. (5):

$$\Delta N = \frac{\chi_{Fe} - \chi_{inh}}{2(\eta_{Fe} + \eta_{inh})} \quad (5)$$

χ_{inh} and χ_{Fe} represent the absolute electronegativities of the corrosion inhibitor and iron, respectively. η_{Fe} and η_{inh} denot the absolute hardness of iron and the corrosion inhibitor, respectively. The theoretical value of η_{Fe} was 0 eV·mol⁻¹. The theoretical value of χ_{Fe} was 7.0 eV/mol. The η_{inh} and χ_{inh} could be computed via the following formulas Eqs. (6-11):

$$I = -E_{HOMO} \quad (6)$$

$$A = -E_{LUMO} \quad (7)$$

$$\chi = \frac{I + A}{2} \quad (8)$$

$$\eta = \frac{I - A}{2} \quad (9)$$

$$\sigma = \frac{1}{\eta} \quad (10)$$

$$\omega = \frac{\chi^2}{2\eta} \quad (11)$$

I stands for ionization potential, A for electron affinity, σ for absolute softness, and ω for the electrophilicity index.

2.7. Surface analysis of QS

QS samples were characterized using Sigma Gemini 300 SEM (Zeiss, VERTEX70 instrument), JC2000DM Contact Angle Measuring Instrument (Shanghai Zhongchen Digital Technology Equipment Co., Ltd.), AXIS SUPRA XPS (Shimadzu, Japan), and MFP-3D Origin AFM (Oxford Instruments, UK), to demonstrate that the synergistic effect of OPE and KI could effectively reduce the corrosion of QS in acidic environments.

3. Results and Discussion

3.1. FTIR and UV-vis spectra analysis of OPE

The FTIR spectra of OPE, hesperidin, and flavone were presented in Figure 1(a). By comparing the infrared spectra of OPE with those of hesperidin, flavone, and their mixtures, it was seen that the infrared spectral pattern of OPE was like that of the mixture of hesperidin and flavonoids, indicating that the main chemical components of OPE were hesperidin and flavonoids [20]. In the infrared spectrum of OPE, due to the influence of the glycoside and glycoside hydroxyl groups, the carbonyl group's (C=O) stretching vibration peak was diminished to 1646.77 cm⁻¹ (it should have been between 1800 and 1700 cm⁻¹ if unaffected). The absorption peak at 3392.68 cm⁻¹ corresponded with the O-H bond's stretching vibration [23]. The medium-intensity absorption peak at 2927.16 cm⁻¹ was the stretching vibration of the C-H bond. The peaks at 1516.32 cm⁻¹ and 1447.32 cm⁻¹ corresponded to the vibrations of double bonds or the C=C of benzene rings. The medium-intensity absorption peak at 1053.40 cm⁻¹ was caused by the stretching vibration of the ether bond C-O-C or the asymmetric vibration of cyclic ether. The range of 923.06-778.55 cm⁻¹ was attributed to the bending vibrations of C-H in olefins, aromatic hydrocarbons, and aldehydes. The FTIR findings suggested that OPE comprised a multitude of polar groups of unsaturated organic compounds, such as hydroxyl, carbonyl, and ether bonds. Organic compounds with these functional groups are suitable for utilization as metal acid wash corrosion inhibitors [20]. Therefore, it was preliminarily inferred that OPE had certain corrosion inhibition properties.

The UV-vis spectra of OPE, hesperidin, and flavone are depicted in Figure 1(b). The UV-vis spectra of the mixture of OPE with hesperidin and flavone were similar. Typically, flavonoids have characteristic absorption peaks in the ultraviolet range of 300 to 400 nm. Hesperidin has characteristic absorption peaks in the 212 nm. In the OPE curve of Figure 1(b), two peaks were observed at 209 nm and 331 nm. The weaker band at 331 nm was caused by the electron leaps of the benzene ring in the cinnamoyl group and flavonoid compounds. The larger absorption peak at 209 nm was due to the electronic transition from n→σ* involving electrons of N and O atoms [24]. The results indicated that the main components of OPE were flavonoids and other compounds containing polar elements like N or O. The structural formula of the main component hesperidin in OPE and the simplified flavone structure are shown in Figure 1(c-d).

3.2 Theoretical Calculation of OPE Molecular Structure

Based on previous reports [20-22] and in conjunction with the results of FTIR and UV-vis in Section 3.1. It was determined that the main components of OPE were hesperidin and flavonoid compounds. Building on the previous research achievements of our research group [22], theoretical calculations examined the correlations between the molecular structure of hesperidin and flavonoids and their corrosion inhibiting ability. Figure 2(a-d) shows the energy levels of the HOMO and lowest unoccupied molecular orbital (LUMO) for the optimized structures of hesperidin and flavonoids. From Figure 2(a-d), it was concluded that HOMO was predominantly localized on the aromatic

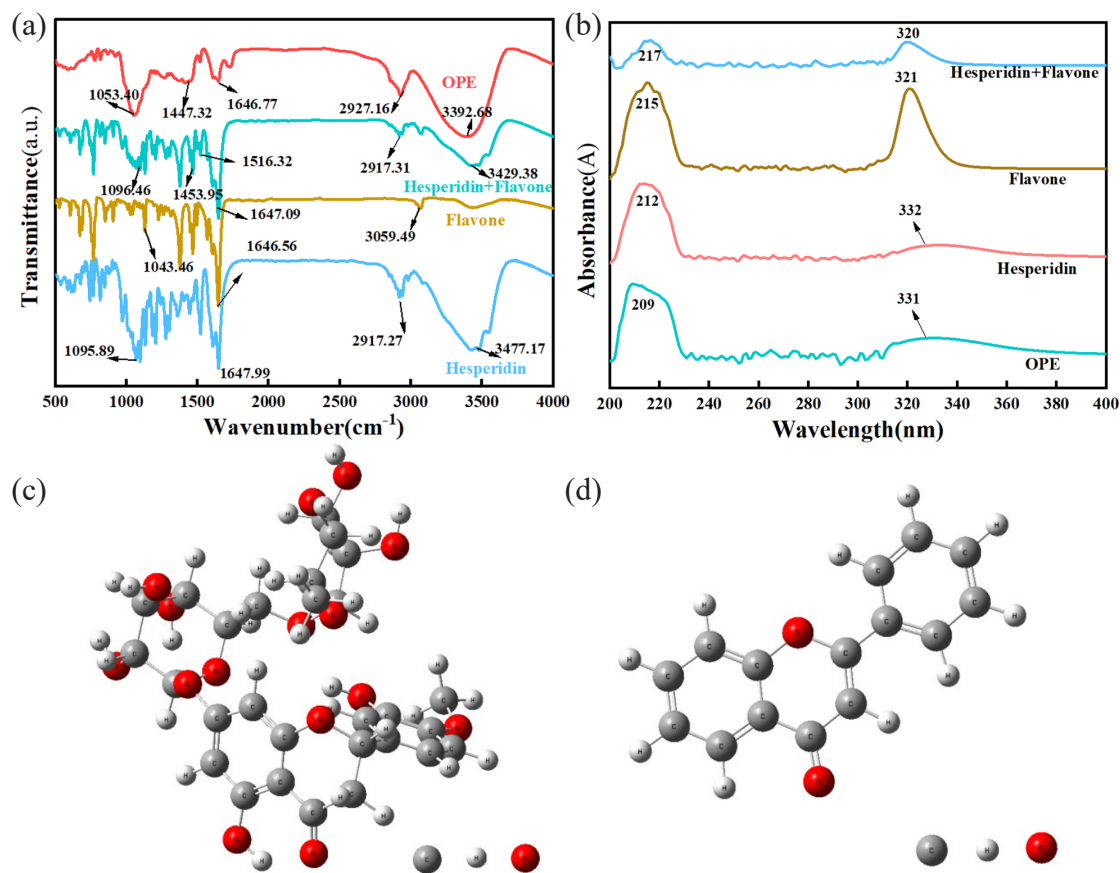


Figure 1. (a) Fourier transform infrared spectroscopy (FTIR) diagram and (b) UV-vis diagram of orange peel extract (OPE), Hesperidin and Flavone, Structural formula of (c) hesperidin and (d) flavon in OPE.

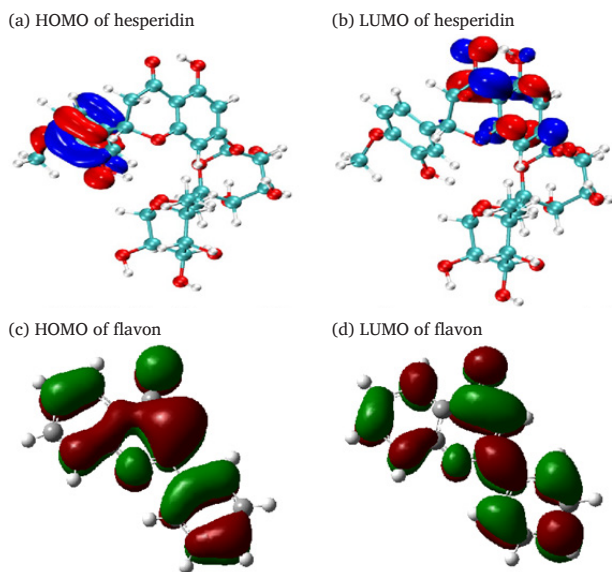


Figure 2. (a-d) HOMO and LUMO orbitals of Hesperidin and flavon. MO: Molecular orbital.

rings, carbonyl, and hydroxyl groups. While LUMO was mainly located at the O-containing heterocycle and benzene ring. Generally, the lower the band gap value of a corrosive inhibitor, the easier is its adsorption on the metallic surface [25]. This would mean a superior protective effect on the metal. Owing to the presence of a dense electron-rich region around the oxygen atoms in the HOMO orbitals of hesperidin and flavone, the lone-pair electrons on the oxygen atoms formed

Table 1. Quantum chemical parameters for Hesperidin and flavonoid.

Inhibitor	E_{HOMO} (eV)	E_{LUMO} (eV)	ΔE (eV)	I	A	χ	η	σ	ω	ΔN
Hesperidin	-5.771	-1.890	3.881	5.771	1.890	3.830	1.941	0.515	3.780	0.817
Flavon	-6.607	-2.112	4.495	6.607	2.112	4.359	2.248	0.445	4.228	0.587

covalent bonds with the empty d-orbitals of iron atoms, to enable the adsorption of hesperidin and flavonoids on the QS surface. As shown in Table 1, the molecules of hesperidin and flavonoids possessed higher E_{HOMO} , lower E_{LUMO} , and ΔE values. This provided a theoretical basis for OPE's effectiveness in preventing QS corrosion in HCl environments. Meanwhile, the electron transfer numbers for hesperidin and flavon were 0.817 and 0.587, respectively, both positive. This indicated that electrons transfer occurred from hesperidin and flavon to iron atoms. Electron exchange between hesperidin, flavonoids, and iron surfaces aided in the formation of coordination bonds with iron, which enhanced chemical adsorption. The ω was a measurement of the electron-attracting capacity of molecules or atomic groups. For corrosion inhibitors, a higher electrophilic index was indicative of a greater capacity to attract electrons. The reason for this was that the OPE interacted with the QS surface through their electrophilic centers such as -OH, aromatic rings, and C=O, forming a stable adsorption layer. This effectively prevented QS from contacting the corrosive agent, achieving the suppression effect. Hesperidin and flavon, which contained many aromatic rings and hydroxyl groups, had a high electrophilic index. They exhibited robust adsorption properties on the metallic surface.

3.3. Weight loss method measurement

3.3.1. Corrosion inhibiting efficiency of OPE or KI

Utilizing the weight loss method, this research first assessed the corrosion inhibiting ability of OPE and KI as inhibitors in HCl

environments separately. In Figure 3(a), η_w gradually raised with increasing OPE content in the HCl environments. The η_w was 80.16% when the OPE concentration was 0.8 g/L. Therefore, OPE could reduce the corrosion of QS in HCl environments, but the corrosion inhibiting ability of OPE still needed to be improved. From Figure 3(b) it could be seen that η_w increased with the increase in KI content. The maximum η_w was 30.87% and 35.68% when the concentration of KI reached 0.1 g/L and 0.2 g/L, respectively. Therefore, the corrosion inhibiting ability of KI was weak. To enhance the corrosion inhibition of OPE and KI, this study combined OPE with KI to leverage their synergistic corrosion inhibiting abilities, thereby improving the overall corrosion inhibiting performance. Due to the high cost of KI, its concentration ought to be maintained at the lowest possible level. Thus, as shown in Table 2, based on the corrosion inhibiting efficiency of KI reported in existing literature, the ideal concentration of KI was determined to be 0.1 g/L and different contents of OPE were added to ascertain corrosion inhibiting ability of the OPE/KI system.

3.3.2. The synergistic corrosion inhibiting ability of OPE and KI

To enhance the corrosion inhibiting efficiency, KI was optimally used at a concentration of 0.1 g/L in combination with varying contents of OPE (0.2 g/L to 0.8 g/L). Through weight loss experiments, the η_w of the OPE/KI composite system at different temperatures and different OPE contents was shown in Table 3. It was apparent that compared to the individual corrosion inhibiting efficiency of using OPE or KI, the OPE/KI exhibited excellent corrosion inhibiting ability. Table 3 indicated that the corrosion inhibiting ability rose alongside the content of OPE at a certain temperature. This was because as the OPE content increased, more OPE was adsorbed onto the QS surface, creating an adsorbent film. The protective film formed by OPE / KI on the QS effectively prevented the invasion of corrosive environments, which reduced the corrosion of QS [26]. Table 3 showed that the corrosion inhibiting performance was optimal at a content of 0.8g/L OPE/0.1g/L KI. The corrosion inhibition efficiency reached as high as 97.05%. This result was compared to the previously summarized research findings on the combined use of plant extracts and KI in Table 2 [27-31]. The synergistic effects of 0.8g/L OPE / 0.1g/L KI showed broad application prospects in delaying the corrosion of QS in hydrochloric acid systems. Meanwhile, when the OPE concentration was constant, the corrosion inhibiting efficiency dropped with increase in temperature. This was mainly due to change in the dissociation and adsorption equilibrium of the OPE/KI in the solution under different temperature conditions, leading to a reduction in the corrosion inhibiting ability [32]. From 20°C to 30°C, the corrosion inhibiting efficiency (η_w) of the corrosion inhibitor at a concentration of 0.8g/L OPE/0.1g/L KI decreased from 97.05% to 89.02%. This suggested that the corrosion inhibiting efficiency remained largely unaffected by temperature fluctuations. Therefore, the combined use of OPE and KI had a certain adaptability to temperature. And OPE/

Table 2. Comparison of inhibition efficiency (η_w) of OPE/KI with the literature data of previous reports about the synergistic inhibition of plant extracts with KI for steel in acid solutions.

Plant extract	c (extract)	c (KI)	Acid	η_w	Refs
<i>Mikania micrantha</i> extract	0.1g/L	0.1g/L	0.5M H ₂ SO ₄	94.4%	[27]
rubber seed extract	0.2g/L	0.1g/L	0.5M H ₂ SO ₄	96.4%	[28]
<i>Mikania micrantha</i> extract	0.1g/L	0.1g/L	0.1M methanesulfonic acid	91%	[29]
Camellia Oleifera shell extract	0.4g/L	0.02g/L	0.5M H ₂ SO ₄	93.08%	[30]
Michelia alba leaf extract	0.8g/L	0.4g/L	0.5M H ₂ SO ₄	95.02%	[31]

OPE: Orange peel extract, KI: Potassium iodide.

Table 3. Synergistic inhibition effects of OPE at various content and 0.1g/L KI on QS in 0.5 M HCl.

Temperature /°C	OPE / (g/L)	$V_{\text{rate}}/10^{-4}(\text{g}/\text{cm}^2 \cdot \text{h})$	η_w (%)
20	0	3.484	/
	0.1	1.616	53.62
	0.2	0.717	79.42
	0.4	0.382	89.05
	0.6	0.179	94.87
	0.8	0.103	97.05
30	0	11.05	/
	0.1	6.289	43.83
	0.2	2.726	74.02
	0.4	1.926	85.57
	0.6	1.102	90.03
	0.8	0.556	94.98
40	0.8	3.053	92.01
50	0.8	10.16	89.02

OPE: Orange peel extract, KI: Potassium iodide, QS: Q235 steel.

KI worked as a high efficiency and environmentally friendly anti-corrosion agent. To assess the potential synergism between OPE and KI, the synergistic coefficient was determined using formula Eq. (12) [33]:

$$s = \frac{1 - \eta_A - \eta_B + \eta_A \eta_B}{1 - \eta_{AB}} \quad (12)$$

In the text, η_A and η_B represented the corrosion inhibiting efficiencies of OPE and KI when used alone in the inhibition system, respectively. And η_{AB} was the corrosion inhibiting efficiency value of the OPE/KI complex system. An s value exceeding 1 signified a synergistic interaction between OPE and KI. A value of $s < 1$ indicated an antagonistic effect between OPE and KI. $s = 1$ indicated no interaction between OPE and KI [34]. As shown in Figure 4, an upward trend in 's' was observed with

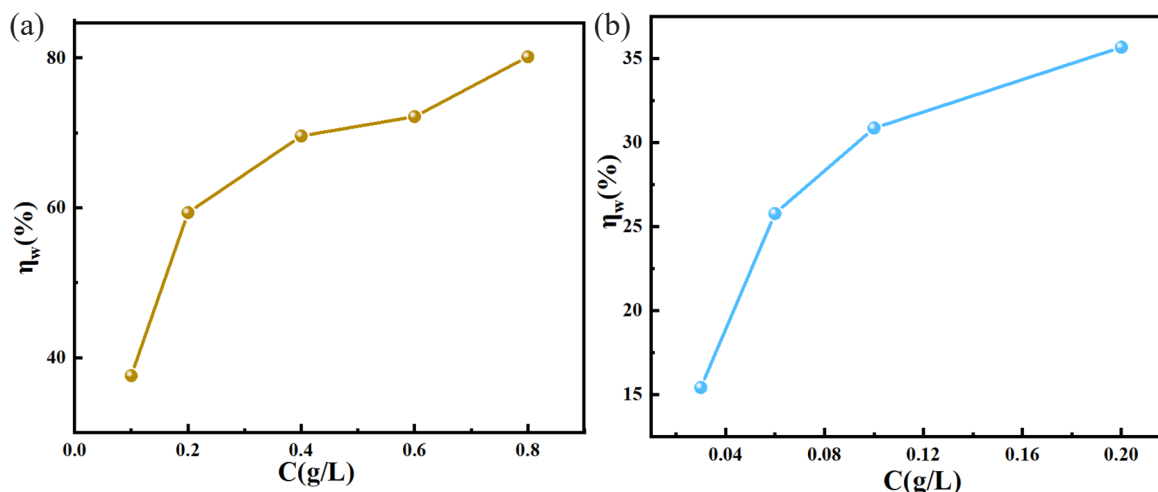


Figure 3. Corrosion inhibiting efficiency (η_w) versus orange peel extract (OPE) (a) or potassium iodide (KI) (b) concentration in 0.5M HCl.

increasing concentrations of OPE/KI at 30°C. When the content of OPE was more than 0.1 g/L, 's' was more than 1. This suggested a synergistic interaction between OPE and KI. The highest 's' value at 0.8g/L OPE indicated that the synergistic effect of the complex system of 0.8g/L OPE and 0.1g/L KI was the most outstanding.

3.3.3. Adsorption isotherms of OPE/KI

The synergistic effect of OPE/KI was influenced by their adsorption performance on the QS surface [35]. This study utilized the Langmuir adsorption isotherm to model the adsorption behavior of OPE/KI on the QS surface [36].

$$\frac{c}{\theta} = \frac{1}{K_{ads}} + c \quad (13)$$

In Eq. (13), c denoted the corrosion inhibitor's content in g/L, θ signified the surface coverage, and K_{ads} was the adsorption equilibrium constant. Figure 5 displayed the linear fitting curve for OPE/KI. The associated linear regression parameters and K_{ads} are displayed in Table 4. The closeness of R^2 to 1 for OPE/KI implied that the adsorption of OPE/KI onto the QS surface adhered to the Langmuir adsorption isotherm. The slope values of the fitted line deviated from 1, suggesting that there were interactive forces between the adsorbed molecules. In comparison, the slope at a temperature of 20°C for the OPE/KI complex system was closer to 1, indicating that the interactive forces between OPE and KI were weaker at lower temperatures. Moreover, Table 4 shows that K_{ads} was highest at 20°C, so the interaction of OPE/KI with the QS surface was strongest at this temperature. The corrosion inhibiting efficacy of OPE/KI was optimal at 20°C. As the temperature rose, the value of K_{ads} decreased, and the corrosion inhibitor's adsorption on the QS surface diminished, resulting in a minor decrease in corrosion inhibiting efficacy.

3.3.4. Adsorption thermodynamic parameters of OPE/KI

By calculating the thermodynamic parameters of adsorption, the adsorbing behavior of OPE/KI at the QS surface was further investigated. The Van Hoff equation was as follows [37]:

$$\ln K = -\frac{\Delta H_{ads}^0}{RT} + \frac{\Delta S_{ads}^0}{R} - \ln C_{H_2O} \quad (14)$$

ΔH_{ads}^0 represented the standard enthalpy of absorption in kJ/mol. K denoted the equilibrium constant for absorption. R was the ideal gas

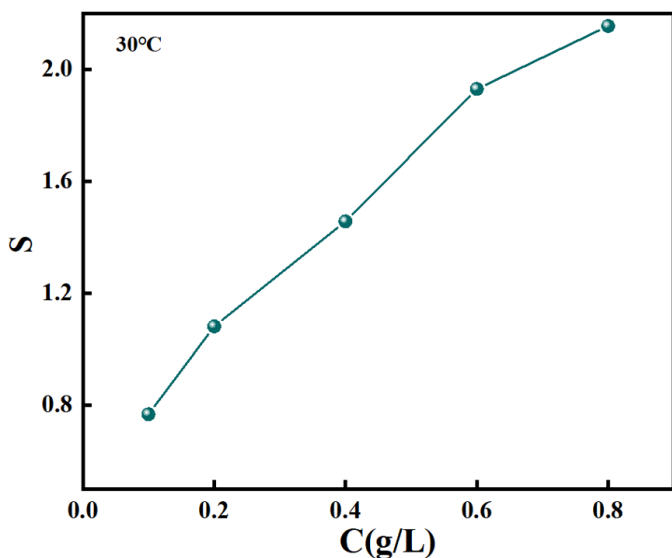


Figure 4. The synergy coefficient (S) of various contents of OPE and 0.1g/L KI on Q235 steel (QS) in 0.5M HCl.

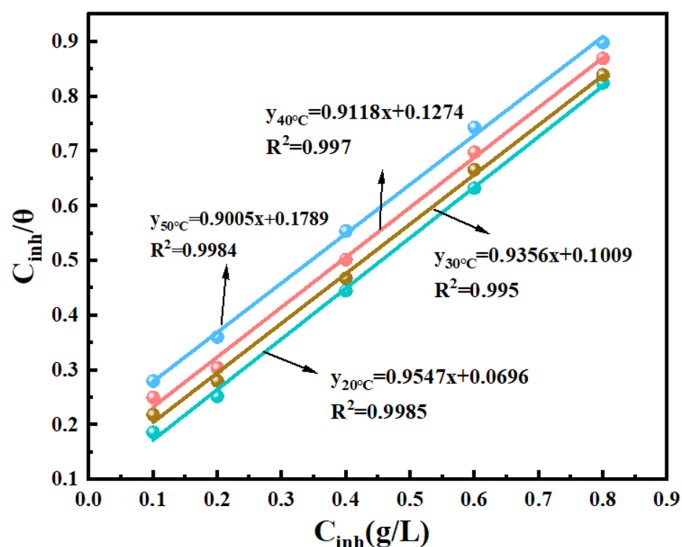


Figure 5. Langmuir adsorption isotherm of Q235 steel (QS) in orange peel extract (OPE)/potassium iodide (KI) composite system.

Table 4. Linear regression parameters of fitted Langmuir adsorption isotherm.

Temperature (K)	K_{ads} (L/g)	Slope	R^2
293	14.37	0.9547	0.9985
303	9.91	0.9356	0.9950
313	7.85	0.9118	0.9970
323	5.59	0.9005	0.9984

constant equal to 8.314 J/k·mol. C_{H_2O} was taken as approximately 10^3 g/L. T stood for the temperature in Kelvin. Based on Eq. (14), the linear relationship between $\ln K$ and $1/T$ is depicted in Figure 6. The slope of the fitted line was $\Delta H_{ads}^0/R$ and the intercept gave ΔS_{ads}^0 . The Gibbs free energy (ΔG_{ads}^0) was determined by Eq. (15) [38].

$$\Delta S_{ads}^0 = \frac{\Delta H_{ads}^0 - \Delta G_{ads}^0}{T} \quad (15)$$

The adsorption thermodynamic parameters of ΔH_{ads}^0 , ΔG_{ads}^0 and ΔS_{ads}^0 at 20°C~50°C are shown in Table 5. ΔH_{ads}^0 was negative in HCl solutions containing different concentrations of OPE/KI, which meant that the OPE/KI had released heat during the whole procedure of adsorption to the QS surface. During the exothermic process, the higher the temperature, the weaker was the adsorption capacity. This reduced the corrosion inhibition ability of OPE/KI [39]. In Table 5, ΔG_{ads}^0 was negative at all temperatures, indicating that the adsorption was spontaneous. A ΔG_{ads}^0 value greater than -20 kJ/mol signifies physisorption of the inhibitor and less than -40 kJ/mol signifies chemical adsorption [40]. In corrosive environments, the ΔG_{ads}^0 value for the adsorption of OPE/KI on the QS surface was between -40 kJ/mol and -20 kJ/mol. OPE/KI adsorbed to the QS surface via physical and chemical adsorption processes. The ΔS_{ads}^0 being negative suggested that OPE/KI exhibited a higher degree of freedom and disorder in the solution before adsorption. Upon adsorption onto the QS surface, the increase in intermolecular forces led to a rise in order and a corresponding decrease in disorder [27].

3.3.5. Analysis of dynamic corrosion parameters

This study explored the influence of temperature on the speed of corrosion of QS by assessing the inhibitory effects of OPE at different concentrations in a corrosive environment. Kinetic parameters were calculated utilizing the Arrhenius equation and the transition state theory equation [41].

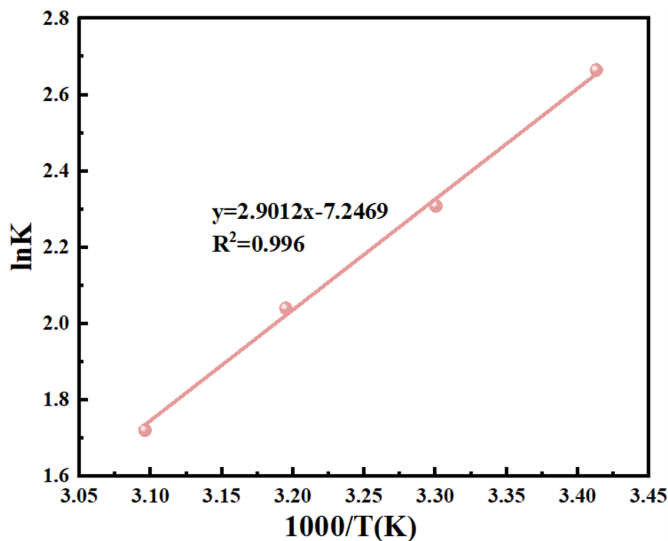
Figure 6. Linear fitting of $\ln K - 1/T$.

Table 5. Absorption thermodynamic parameters of OPE /KI on QS in a corrosive environment.

Temperature (K)	ΔG° ads (KJ/mol)	ΔH° ads (KJ/mol)	ΔS° ads (J/ mol·k)
293	-23.293	-24.12	-2.820
303	-23.266	-24.12	-2.820
313	-23.237	-24.12	-2.820
323	-23.209	-24.12	-2.820

QS: Q235 steel, OPE: Orange peel extract, KI: Potassium iodide.

$$\log v = \frac{-E_a}{2.303RT} + \log A \quad (16)$$

$$\log \frac{v}{T} = \log \frac{R}{Nh} + \frac{\Delta S_a}{2.303R} - \frac{\Delta H_a}{2.303RT} \quad (17)$$

E_a and A in Eq. (16) represented the apparent activation energy and pre-exponential factor, respectively. In Eq. (17), N , h , ΔH_a , and ΔS_a represented Avogadro's number ($6.02 \times 10^{23} \text{ mol}^{-1}$), Planck's constant ($6.626 \times 10^{-34} \text{ J s}$), enthalpy change, and entropy change of the reaction, respectively. Figure 7(a-b) displays the linear fitting curves of $\log v^{-1}/T$ and $\log(v/T)^{-1}/T$ for QS exposed in corrosive solution at 20–50°C. The kinetic parameters varied with the concentration of OPE. And the data are present in Table 6. It could be noted from Table 6 that compared to

Table 6. Thermodynamic parameters of QS soaked in 0.5 M HCl with variable contents of OPE.

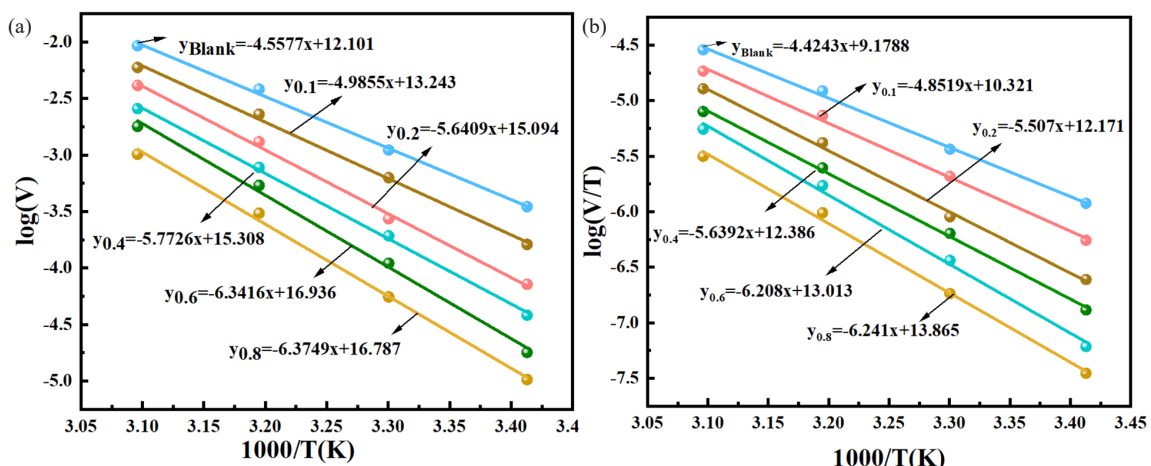
C(g/L)	E_a /(kJ/mol)	ΔH_a /(KJ/mol)	ΔS_a /(J/mol·K)
0	87.267	84.713	-21.82
0.1	95.458	92.900	0.039
0.2	108.001	105.445	35.451
0.4	110.528	107.975	39.566
0.6	121.423	118.965	51.578
0.8	122.061	119.506	67.876

QS: Q235 steel, OPE: Orange peel extract

the blank HCl environments, the E_a values for the corrosive solutions containing OPE/KI were all increased. Moreover, as the content of OPE rose, the E_a values also increased. When different concentrations (0~0.8g/L) of OPE were added to 0.1g/L KI, E_a increased from 84.713 kJ/mol to 122.061 kJ/mol. Consequently, with the rising concentration of OPE, the E_a value also rose, signifying an elevated minimum energy required for the corrosion reaction. The corrosion reaction became more difficult to carry out, thereby reducing the QS corroding in acidic environments. Thus, the inhibitor with a concentration of 0.8g/L OPE/0.1g/L KI exhibited the best corrosion inhibiting ability. Table 6 reveals the positive ΔH_a , suggesting that QS corrosion was an endothermic reaction that needed extra energy to initiate the QS's corrosion. The ΔS_a in the HCl environments containing OPE/KI was positive, while in the blank HCl solution, the ΔS_a was negative. The increased ΔS_a could be due to heightened disorder as the reactants became activated complexes, as well as the repulsion of water molecules when the inhibitor adsorbed onto the QS [42].

3.4. Potentiometric polarization curve testing of OPE/KI

Figure 8 displays the OCP and PDP of QS soaked in a corrosive inhibitory environment. In Figure 8(a), after the QS electrode was exposed to the corrosive inhibitory environment for 1800 s, the OCP gradually leveled off, indicating that the reaction at the QS interface had reached a steady state. Figure 8(b) illustrates that the overall polarization curve of the OPE/KI moved to the lower corroding current densities, which indicated the effectiveness of the OPE/KI system in inhibiting the cathodic and anodic reactions. To further analyze the corrosion inhibiting efficiency and electrochemical corrosion mechanism of QS under different concentrations of the OPE/KI complex system, the PDP curves were fitted. The results obtained are presented in Table 7. Table 7 indicated that the introduction of OPE/KI reduced both cathodic Tafel slope (β_c) and anodic Tafel slope (β_a) when compared to the HCl solution devoid of OPE/KI. And the downward shift of the Tafel curve with increasing OPE concentration suggested that OPE functioned as a mixed-type inhibitor, blocking cathodic as well as anodic reactions [43]. When the content of OPE in the OPE/KI system in the corrosive environment reached 0.8g/L, the i_{cor} decreased

Figure 7. (a) Linear fitting of $\log V^{-1}/T$ in 0.5 M HCl solution, (b) Linear fitting of $\log(V/T)^{-1}/T$ in 0.5 M HCl solution.

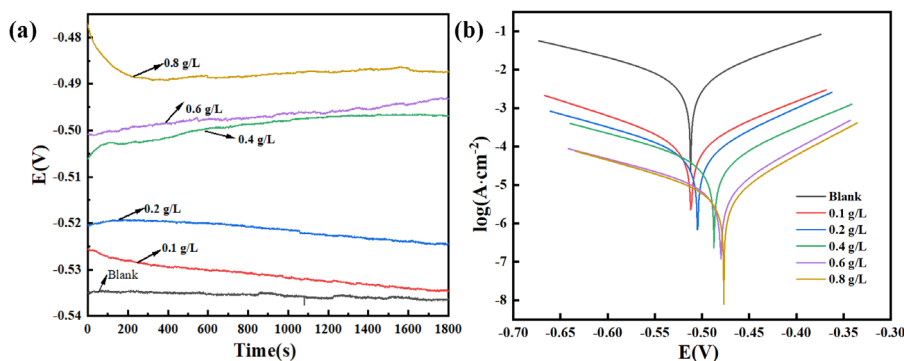


Figure 8. (a) Open circuit potential (OCP) curve and (b) polarization curve of Q235 steel (QS) soaked in 0.5 M HCl with OPE and KI compound system (OPE/KI) for 1800 s at 30°C.

Table 7. Potentiodynamic polarization curve parameters of QS in system with OPE/KI.

C_{inh} (g/L)	E_{cor} (mV)	i_{cor} (mA/cm ²)	β_a (mV/dec)	β_c (mV/dec)	η (%)
0	-512	6.401	129	179	/
0.1	-512	3.822	110	160	40.29
0.2	-505	1.475	92.9	158	76.96
0.4	-487	0.959	90.2	156	85.02
0.6	-480	0.432	85.1	150	93.25
0.8	-477	0.203	78.0	146	96.82

QS: Q235 steel, OPE: Orange peel extract, KI: Potassium iodide.

from 6.401 mA/cm² to 0.203 mA/cm², and η was as high as 96.82%. This was essentially consistent with the results of the weightlessness method. The polar groups in OPE were adsorbed on the QS surface through interactions with iron, reducing the QS's exposed area in the corrosive environments [44]. Furthermore, the presence of KI enhanced OPE adsorption onto QS, leading to more effective corrosion inhibition in acidic environments and boosting the corrosion inhibiting ability.

3.5. EIS testing of OPE/KI

EIS was a direct and efficient method of estimating the anti-corrosion properties of materials. Figure 9(a-c) respectively shows the Nyquist plot, Bode plot, and the equivalent circuit diagram used to fit the data from EIS of QS soaked in a 0.5 M HCl which contained varying content of OPE/KI. In Figure 9(a), the Nyquist plot showed that the OPE/KI inhibitor system's capacitive arc resembled the blank corrosive solution's arc. This suggested that incorporating OPE/KI did not change the electrode's electrochemical reaction mechanism. OPE/KI functioned as a corrosion inhibitor by adsorbing on the electrode surface, thereby minimizing metallic corrosion [45]. Figure 9(b) displayed the Bode and phase angle plots of QS soaked in acidic environments containing OPE/KI. The phase angle increased with increasing OPE concentration, but remained below 90°. This suggested that there was a dispersion effect on QS's corrosion in the HCl environment containing OPE/KI [46]. Moreover, the impedance modulus of QS was depicted in Figure 9(b). As the OPE concentration increased, the $\log |Z|$ gradually increased as well. The trends in phase angle and $\log |Z|$ changes confirmed that 0.8 g/L OPE / 0.1 g/L KI provided the best corrosion inhibiting ability for QS in an acidic environment.

To get impedance parameters, the EIS data were evaluated by application of the equivalent circuit model shown in Figure 9(c). The chi-square (χ^2) statistic assessed the fit accuracy of the circuit model, with lower values signifying closer alignment to experimental results. R_s and R_{ct} represented the solution resistance and charge transfer resistance, respectively. The higher the R_{ct} , the harder it became for QS to undergo corrosion reactions in acidic environments. Consequently, the better the corrosion inhibiting ability of OPE/KI. CPE represented the Constant Phase Element and C_{dl} represented the double-layer capacitance. The formula for calculating C_{dl} was presented below (Eq. 18) [47]:

$$C_{dl} = Y_0^n \times R_{ct}^n \quad (18)$$

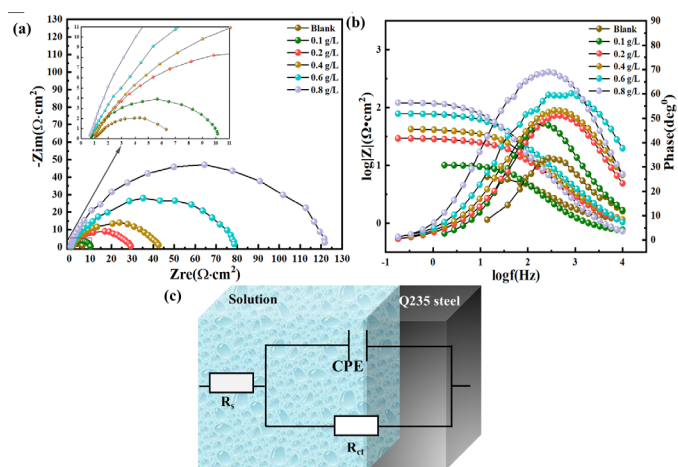


Figure 9. (a) Nyquist diagram of Q235 steel (QS) at 0.5 M HCl with or without orange peel extract (OPE)/potassium iodide (KI), (b) Bode diagram of QS in 0.5 M HCl with or without OPE/KI, (c) Equivalent circuit for fitting Electrochemical Impedance Spectroscopy (EIS) data. CPE: Constant phase element.

Fitting the Nyquist plot and according to Eq. (4), the η was obtained. Table 8 shows that the addition of OPE/KI to a corrosion solution caused a swift rise in charge transfer resistance (R_{ct}). When the content of the corrosion inhibitor was 0.8g/L OPE/ 0.1g/L KI, R_{ct} reached 115.86 $\Omega \cdot \text{cm}^2$. And the η reached up to 95.27%. This further indicated that the 0.8g/L OPE / 0.1g/L KI was effective in reducing the QS's corrosion in HCl environments. Meanwhile, as the content of OPE in OPE/KI increased, the C_{dl} value decreased from 169.65 mF/cm² to 8.27 mF/cm². The decline in C_{dl} was caused by the adsorption of OPE/KI onto the QS surface. This was due to the adsorption of corrosion inhibitors on metal surfaces, which can reduce the local permittivity and increase the bilayer thickness [48]. Values of α below 1 indicated that frequency dispersion existed in corrosive solutions containing OPE/KI across the electrode-solute interface.

3.6. SEM, FTIR, CA and AFM analysis of QS surface

Table 8. Impedance analysis parameters of QS in 0.5 M HCl with or without OPE/KI.

C_{inh} (g/L)	R_s ($\Omega \cdot \text{cm}^2$)	R_{ct} ($\Omega \cdot \text{cm}^2$)	C_{dl} (mF·cm ²)	CPE		χ^2	η (%)
				Y_0 ($\mu\Omega^{-1} \cdot \text{s}^n \cdot \text{cm}^{-2}$)	n		
0	1.033	5.966	169.65	1340.76	0.744	0.0841	/
0.1	0.716	9.891	102.25	993.63	0.811	0.0744	39.68
0.2	0.854	27.663	36.61	500	0.757	0.0403	78.43
0.4	0.835	41.134	24.36	458.59	0.749	0.0364	85.49
0.6	0.577	78.186	12.96	305.09	0.765	0.0501	92.36
0.8	0.593	115.866	8.27	244.27	0.854	0.0769	95.27

QS: Q235 steel, OPE: Orange peel extract, KI: Potassium iodide.

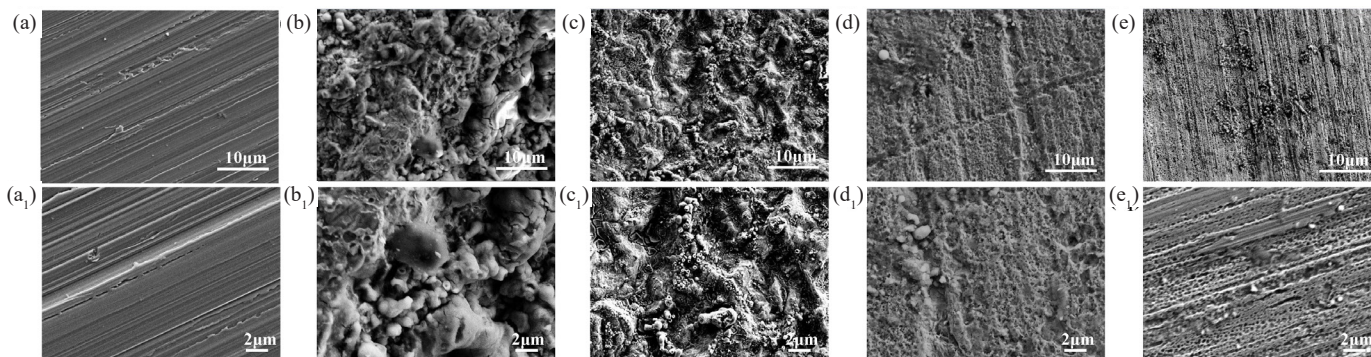


Figure 10. Scanning electron microscopy (SEM) images of Q235 steel (QS): (a, a₁) polished, (b, b₁) in 0.5 M HCl, (c, c₁) in 0.5 M HCl + 0.1 g/L potassium iodide (KI), (d, d₁) in 0.5 M HCl + 0.8 g/L orange peel extract (OPE), (e, e₁) in 0.5 M HCl + 0.8 g/L OPE and 0.1 g/L KI.

SEM was utilized to characterize the micromorphology of the QS corroded area. Figure 10 (a, a₁) presents the polished surface of QS before corrosion. The image shows a smooth QS surface with minor manual-polishing scratches before corrosion. Figure 10 (b, b₁) showed the metal surface of QS after being corroded by blank corrosion solution. From the figure, it can be observed that a large number of corrosion pits and corrosion products had formed on the metal surface after being corroded by HCl. This indicated that QS had suffered severe corrosion in a strongly acidic medium. Figure 10 (c, c₁) and (d, d₁) show the corrosive surfaces of QS after the addition of KI and OPE into the HCl solution, respectively. Compared with QS corroded in blank solution Figure 10 (a, a₁), the surface corrosion degree of QS soaked in corrosive solution containing OPE and KI had reduced. This indicated that both OPE and KI were able to effectively decelerate the rate of corrosion of QS in corrosive environments. Figure 10 (e, e₁) displays the corroded surface of QS after the addition of OPE/KI in corrosive environments. The surface of QS was smooth, showing almost no signs of corrosion. Additionally, the mechanical scratches resulting from manual polishing were clearly visible on the QS surface. This result was attributed to the synergistic effect of OPE and KI, which formed a uniform adsorption film on the metal surface. This effectively blocked direct contact between corrosive substances and metals. Thus, the OPE/KI corrosion inhibition system exhibited excellent corrosion inhibiting ability.

Figure 11 displayed the FTIR spectrum of OPE and the FTIR spectrum of QS after its immersion in an HCl solution containing OPE/KI. The OPE exhibited adsorption peaks at wavenumbers 1053.40 cm⁻¹ (C-O-C), 1646.77 cm⁻¹ (cyclic ether), 2927.16 cm⁻¹ (C-H), and 3392.68 cm⁻¹ (-OH). The QS immersed in the corrosive solution containing OPE/KI showed corresponding adsorption peaks in the infrared spectrum, as seen in Figure 11. Therefore, it was inferred that OPE had established an adsorptive layer on QS's surface, likely owing to the functional groups like oxygen atoms and hydroxyls present in OPE. These groups acted as active sites for interaction with metallic surfaces. This promoted the chemical reaction between the OPE and the QS surface, forming a stable chemisorption layer and inhibiting the QS's corrosion reaction. To achieve the goal of reducing metal corrosion.

The metallic surface hydrophobicity was increased through adsorption by the corrosive inhibitor, which effectively repelled the environment water molecules. Consequently, this research employed a contact angle meter to assess the QS's contact angle after exposure to acidic solution. The results showed in Figure 12(a-e) indicate that the contact angle of uncorroded QS was 95°. The contact angle of QS after corrosion in HCl solution was 68.5°. The contact angle of QS after corrosion in HCl containing KI was 76°. The contact angle of QS after corrosion in HCl environments containing OPE was 80°. And the contact angle of QS after corrosion in HCl environments containing OPE/KI was 90°. Rising contact angle measurements suggested that the steel surface's hydrophobicity escalated upon the introduction of corrosion inhibitors. The OPE/KI adsorbed on the QS surface repelled water molecules, minimizing QS's interaction with water and thus

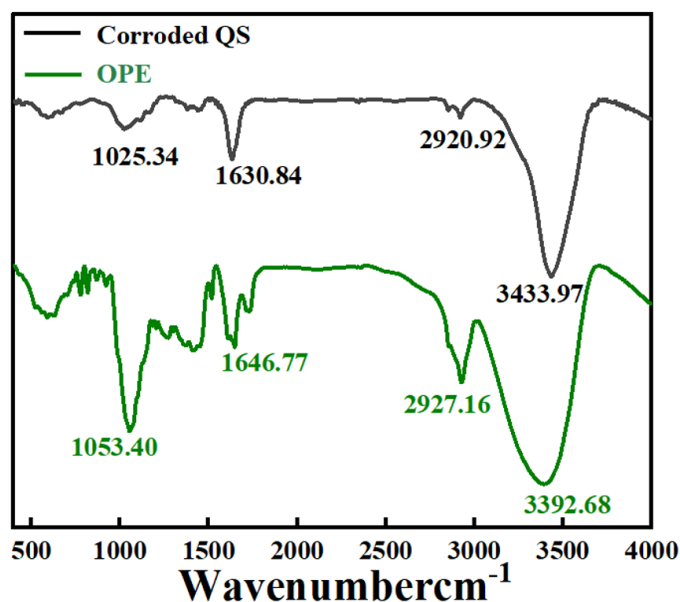


Figure 11. Fourier transform infrared spectroscopy (FTIR) spectrum of orange peel extract (OPE) and the FTIR spectrum of the Q235 steel (QS) after its immersion in an HCl solution containing OPE/potassium iodide (KI).

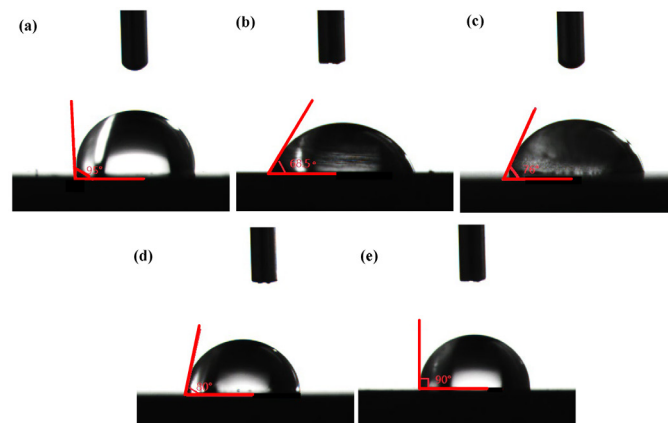


Figure 12. Contact angle (CA) images of (a) polished Q235 steel (QS), (b) QS soaked in 0.5 M HCl, (c) QS soaked in 0.5 M HCl and 0.1 g/L potassium iodide (KI), (d) QS soaked in 0.5 M HCl and 0.8 g/L KI, and (e) QS soaked in 0.5 M HCl and 0.8 g/L OPE and 0.1 g/L KI.

curtailing QS's corrosion. The OPE/KI exhibited excellent corrosion inhibiting ability.

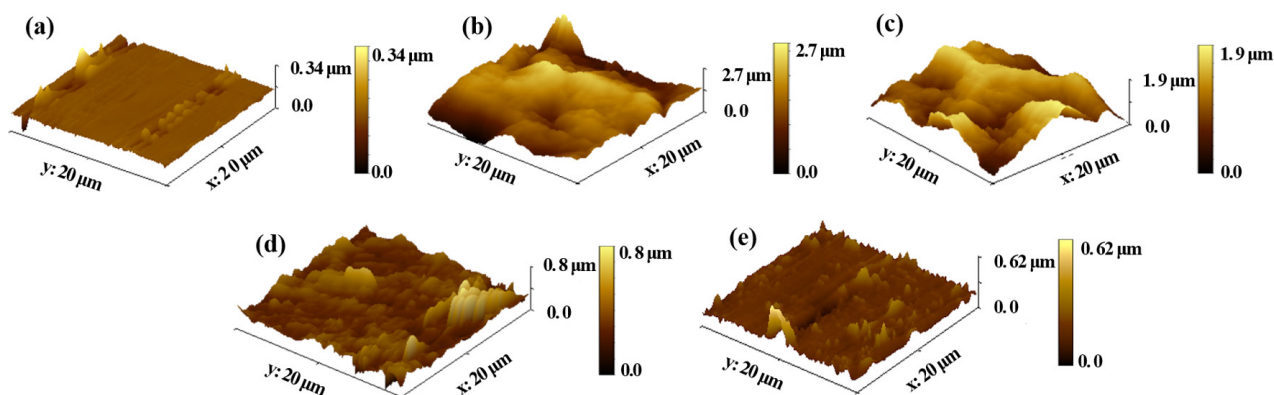


Figure 13. Atomic force microscopy (AFM) images of (a) polished Q235 steel (QS), (b) QS soaked in 0.5 M HCl, (c) QS soaked in 0.5 M HCl and 0.1 g/potassium iodide (KI), (d) QS soaked in 0.5 M HCl and 0.8 g/L OPE, and (e) QS soaked in 0.5 M HCl and 0.8 g/L OPE, and 0.1 g/L KI.

Further observation of the QS surface was done by AFM. The 3D-AFM images of QS are illustrated in Figure 13. According to Figure 13(a), the QS surface that had been hand polished and had not undergone corrosion was flat. But it was not absolutely smooth and uniform, and there were still some small defects on the QS. Figure 13(b) shows the surface of QS corroded in blank acid, where the QS steel surface was severely corroded and had become extremely rough. Figure 13(c) and (d) represented the surfaces of QS with the addition of KI and OPE, respectively. Compared to Figure 13(b), the degree of corrosion at the QS electrode was reduced, and the metallic surface roughness was decreased. Figure 13(e) illustrated the corroded surface of QS with the additive of the OPE/KI. Compared with Figure 13(d), the roughness of the QS surface was lower. This indicated that the OPE/KI mixture had a pronounced inhibitory effect against QS corrosion in acidic environments.

Table 9 presents the average surface roughness (R_a) and root-mean-square roughness (R_q) values, with higher figures indicating increased surface roughness. The polished QS surface, free from corrosion, exhibited the lowest R_a and R_q values. In 0.5M HCl without inhibitors, the QS surface had larger R_a and R_q values. However, the introduction of inhibitors led to a reduction in R_a and R_q values, signifying a substantial corrosion-inhibiting impact on QS in acidic environments. This further confirmed the film-forming property of the inhibitors on the QS [49,50]. Moreover, the R_a and R_q parameters also followed the anticipated regularity: OPE/KI < OPE < KI, thus the compound use of OPE with KI had a superior corrosion inhibiting ability than when used individually.

3.7. XPS analysis of QS after corrosion

When QS was soaked in a corroding environment containing OPE/KI, an adsorbent film formed on the QS surface that diminished the corrosion rate of QS. This film was typically composed of inorganic compounds produced by the corrosion process, organic corrosion inhibitors, and the complexes that formed between these substances and the metal surface. In this experiment, QS was exposed in 0.5M HCl which included OPE/KI for 6 hrs and the corroded steel surface was analyzed by XPS. Figure 14(a) is the full spectrum of the sample. In the full spectrum, peaks of Fe, C, O, and I can be observed. Thus, it was speculated that both OPE and KI could adsorb onto the QS surface forming a protecting layer, delaying the corrosion of QS. On this basis, the three main elements Fe2p, C1s, and O1s were further analyzed to

Table 9. Surface roughness parameters of QS surface.

Test coupon	R_a (nm)	R_q (nm)
Polished QS	1.004	1.596
QS in 0.5M HCl	18.127	21.315
QS in 0.5M HCl with 0.1 g/L KI	15.954	19.038
QS in 0.5M HCl with 0.8 g/L OPE	10.548	13.176
QS in 0.5M HCl with 0.1 g/L KI+0.8 g/L OPE	4.569	5.629

QS: Q235 steel

determine the functional groups that existed in the corrosion-treated QS surface. The spectra at this high resolution have been presented in Figure 14(b-d). In the Fe2p spectrum of Figure 14(b), characteristic peaks of FeOOH, FeCl₂, Fe₂O₃, and Fe were detected at 724.3 eV, 715.1 eV, 710.6 eV, and 706.8 eV, respectively. Characteristic peaks of Fe(II) and Fe(III) were detected at 719.6 eV and 731.8 eV, respectively, indicating that QS was in an oxidized state during the corrosion process [13,51]. As shown in Figure 14(c), the C1s spectrum had a characteristic peak at 288.5 eV representing C=O. The characteristic peak at 286.6 eV represented C-OH or C-O-C. The characteristic peak at 284.9 eV corresponded to C-H or C-C [13,51]. The O1s spectra (Figure 14d) the characteristic peaks of O²⁻, FeOOH, C-O or H₂O were detected at 529.1 eV, 531.0 eV, 532.5 eV, respectively [13,51,52]. The O²⁻ may have been related to the formation of iron oxide corrosive products. The oxygen in FeOOH likely stemmed from the oxygen present in -OH or C=O. The C-H, C-O, and C=O all came from OPE. Clearly, the XPS and FT-IR test outcomes aligned.

3.8 Synergistic inhibition mechanism of OPE and KI

As hydrochloric acid is a potent acid, it separates completely into H⁺ and Cl⁻ ions in water: HCl = H⁺ + Cl⁻. QS was soaked in an HCl solution. The formation of H₂ at the surface was observed, indicating that the chemical reaction occurring was hydrogen evolution corrosion of QS in HCl: 2H⁺ + 2e⁻ = H₂. This reaction's mechanism encompassed three stages: the Volmer adsorption, Heyrovsky deabsorption, and Tafel recombination processes[53].

$\text{Fe} + \text{H}_3\text{O}^+ + \text{e}^- = \text{FeH}_{\text{ad}} + \text{H}_2\text{O}$; $\text{FeH}_{\text{ad}} + \text{H}_3\text{O}^+ + \text{e}^- = \text{Fe} + \text{H}_2 + \text{H}_2\text{O}$; $\text{FeH}_{\text{ad}} + \text{FeH}_{\text{ad}} = 2\text{Fe} + \text{H}_2$. These three reactions did not occur in isolation but are interconnected. The corrosion inhibitor primarily affected the formation of FeH_{ad}, thereby providing protection against corrosion. The anodic reaction that took place at the QS surface is: $\text{Fe} = \text{Fe}^{2+} + 2\text{e}^-$. When QS was soaked in the solution, it was immediately corroded by Cl⁻: $\text{Fe} + \text{Cl}^- = \text{FeCl}_2$. Additionally, QS might also undergo the following reaction with water molecules [51].

$\text{Fe} + \text{H}_2\text{O} = \text{Fe}(\text{H}_2\text{O})_{\text{ads}}$; $\text{Fe}(\text{H}_2\text{O})_{\text{ads}} = \text{Fe}(\text{OH})_{\text{ads}} + \text{H}^+$; $\text{Fe}(\text{OH})_{\text{ads}} = \text{Fe}(\text{OH})_{\text{ads}} + \text{e}^-$. The above reactions summarize as: $\text{Fe} + \text{H}_2\text{O} = \text{Fe}(\text{OH})_{\text{ads}} + \text{e}^- + \text{H}^+$. The complex ion (FeOH)_{ads} released an electron to form the (FeOH)⁺ ion: $\text{Fe}(\text{OH})_{\text{ads}} = \text{Fe}(\text{OH})^+ + \text{e}^-$. Secondly, it was transformed into the following reaction: $\text{Fe}(\text{OH})^+ + \text{H}^+ = \text{Fe}^{2+} + \text{H}_2\text{O}$.

Upon incorporating OPE, the corrosion degree of QS was reduced. This was attributed to the polar groups (-OH, C=O) within OPE, which were readily protonated in acidic environments. $\text{OPE} + \text{cH}^+ = \text{OPE}_c^+$. So, in the corrosion environment, OPE might have existed in the form of OPE or OPE_c⁺. On one hand, across the entire QS surface, OPE could coordinately bind with Fe atoms through the free electron pairs of oxygen to form chemical adsorption. On the other hand, OPE_c⁺ could be physically adsorbed onto negatively charged anion layers. The presence of Cl⁻ had an inhibitive effect on the adsorbability of the corrosion inhibitor at the steel/corrosion interface. Consequently, in a 0.5 M HCl solution, OPE exhibited only a moderate corrosion inhibition effect on QS. When KI was added, I was oxidized by the oxygen dissolved in the

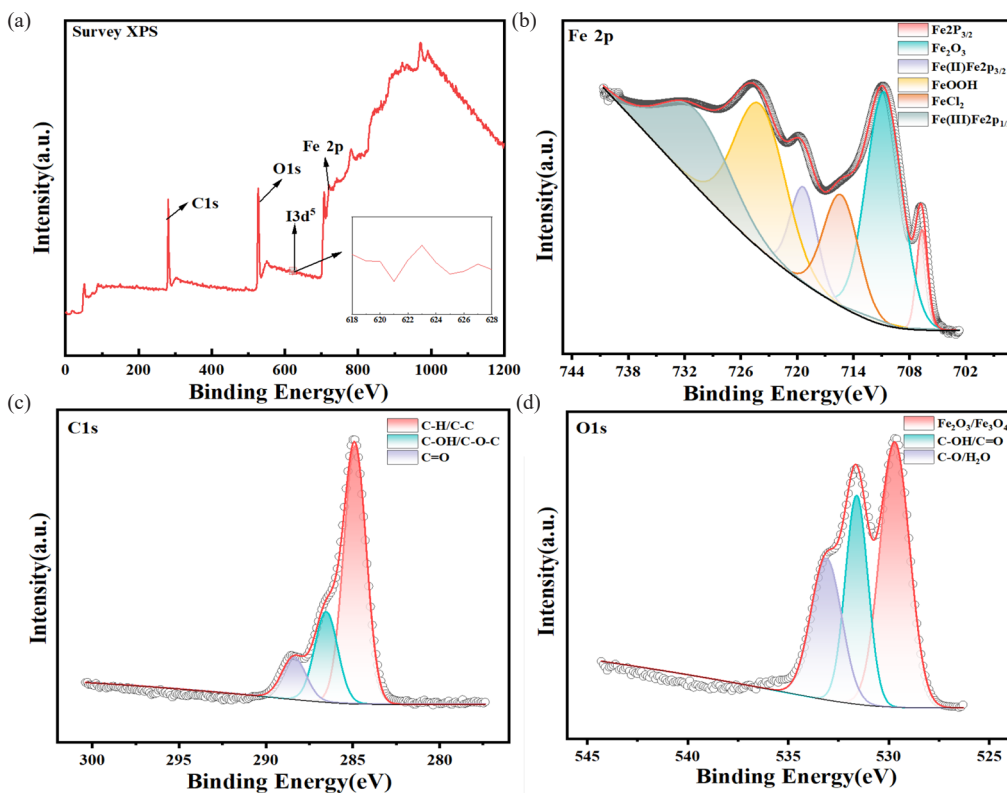


Figure 14. (a) Full spectrum of Q235 steel (QS) soaked in hydrochloric acid containing 0.8g/L OPE and 0.1g/LKI; (b) X-ray photoelectron spectroscopy (XPS) high-resolution spectra of Fe2p, (c) C1s and (d) O1s.

acidic medium to form a pale-yellow triiodide. The iodide ion oxidation process corresponded to the following reaction [27]: $4I^- + 4H^+ + O_2 = 2I_2 + 2H_2O$; $I_2 + I^- = I_3^-$. These two reactions could be summarized as: $6I^- + 4H^+ + O_2 = 2I_3^- + 2H_2O$. During this process, I_3^- would slowly accumulate and be adsorbed at the interface of QS and the solution. Thereby, it played the role of corrosion inhibition. For corrosion systems containing OPE/KI, the strong steric hindrance effect of flavonoids in OPE might limit their adsorption on metal surfaces [29]. Thereby, this affected the performance of OPE as a corrosion inhibitor. The adsorption of I^- or I_3^- on the QS surface could generate a significant amount of negative charge, which was favorable for the adsorption of positively charged OPE_c^{c+} on the metal surface. This promoted the physical adsorption of OPE on the metal surface. Therefore, in this study, we added KI to facilitate the adsorption of OPE_c^{c+} on the QS surface. Secondly, when protonated OPE was closely adsorbed to the metal surface, the polar atoms in OPE (such as oxygen) with lone pairs of electrons could form coordination bonds with metal atoms on the metal surface. This was a mechanism of chemical adsorption. Thus, OPE forms a protective film on the metal surface through both physical and chemical adsorption, thereby reducing the corrosion of the metal.

4. Conclusions

- (1) Theoretical calculations confirmed that hesperidin and flavonoid compounds in OPE could effectively reduce the corrosion of QS in 0.5 M HCl.
- (2) In the corrosive solution, OPE and KI both inhibited QS corrosion, but with relatively low inhibition efficiency. A corrosion inhibiting efficiency of 97.05% was achieved with 0.8g/L OPE/0.1 g/L KI. The synergistic effect of OPE and KI reduced the corrosion of QS in a 0.5 M HCl environment. At the same time, it was demonstrated through thermodynamic parameters that OPE/KI adsorbed to the QS surface via physical and chemical absorption processes.
- (3) Electrochemical tests showed that OPE/KI decreased QS corrosion by suppressing cathodic and anodic reactions, and 0.8g/L OPE / 0.1

g/L KI exhibited the most efficacious anticorrosion effect on QS in hydrochloric acid solution.

- (4) The formation of an adsorbent film on the QS surface by OPE/KI was verified by SEM, FTIR, CA, XPS, and AFM. This adsorbent film served to inhibit the corrosion of the QS.

CRedit authorship contribution statement

Xinhua Liu: Writing – review & editing, Funding acquisition, Formal analysis, Data curation, Conceptualization. **Siyu Liu:** Writing –original draft, Data curation, Formal analysis. **Hongxia Zhang:** Formal analysis. **Yuan Zhang:** Formal analysis, Data curation, Conceptualization. **Baojing Luo:** Formal analysis. **Ying Wang:** Writing – review & editing, **Xiaoyan Xu:** Data curation. **Jiarui Du:** Data curation. **Boxi Yang:** Data curation. **Linyan Gu:** Data curation. **Xingdi Zhao:** Data curation. **Hengyong Wei:** Software.

Declaration of competing interest

The authors declare that they have no known competing financial interests or personal relationships that could have appeared to influence the work reported in this paper.

Declaration of Generative AI and AI-assisted technologies in the writing process

The authors confirm that there was no use of Artificial Intelligence (AI)-Assisted Technology for assisting in the writing or editing of the manuscript and no images were manipulated using AI.

Acknowledgment

The authors acknowledge financial support from the Natural Science Foundation of Hebei Province (D2022105004), Tangshan Normal College key training project (ZDPY07).

References

- Mao, T., Huang, H., Liu, D., Shang, X., Wang, W., Wang, L., 2021. Novel cationic Gemini ester surfactant as an efficient and eco-friendly corrosion inhibitor for carbon steel in HCl solution. *Journal of Molecular Liquids* **339**, 117174. <https://doi.org/10.1016/j.molliq.2021.117174>
- Abdallah, M., Altass, H.M., Al-Gorair, A.S., Al-Fahemi, J.H., Jahdaly, B.A.A.L., Soliman, K.A., 2021. Natural nutmeg oil as a green corrosion inhibitor for carbon steel in 1.0 M HCl solution: Chemical, electrochemical, and computational methods. *Journal of Molecular Liquids* **323**, 115036. <https://doi.org/10.1016/j.molliq.2020.115036>
- Sharma, S., Kumar, A., 2021. Recent advances in metallic corrosion inhibition: A review. *J. Mol. Liq.* **322**, 114862. <https://doi.org/10.1016/j.molliq.2020.114862>
- R Holla, B., Mahesh, R., Manjunath, H., Anjanapura, V., 2024. Plant extracts as green corrosion inhibitors for different kinds of steel: A review. *Heliyon* **10**, e33748. <https://doi.org/10.1016/j.heliyon.2024.e33748>
- Aourabi, S., Driouch, M., Kadiri, M., Mahjoubi, F., Sfaira, M., Hammouti, B., Emran, K.M., 2020. Valorization of Zea mays hairs waste extracts for antioxidant and anticorrosive activity of mild steel in 1 M HCl environment. *Arabian Journal of Chemistry* **13**, 7183-7198. <https://doi.org/10.1016/j.arabjc.2020.08.001>
- Bhaskara, S., Fakrudeen, S.P., Raju, V.B., Murthy, H.C.A., Raghu, A.V., 2021. Comparative studies of inhibitive effects of diamines on corrosion of aluminium alloy in presence of acid media. *Rasayan Journal of Chemistry* **72-82**. <https://doi.org/10.31788/rjc.2021.1456561>
- Lin, B-lan., Zhou, X-xin., Duan, T-hu., Zhao, C., Zhu, J-hao., Xu, Y-ye., 2024. Experimental and theoretical study on corrosion inhibition and adsorption performance of Ipomoea batatas L. leaf extract for mild steel. *Arabian Journal of Chemistry* **17**, 105410. <https://doi.org/10.1016/j.arabjc.2023.105410>
- Radouane, M., Aida, Z., Atmane, D., Amoura, D., Martemianov, S., Thomas, A., Alrashdi, A.A., Makhloufi, L., Lgaz, H., Dib, A., Chafiq, M., Ko, Y.G., 2023. Experimental assessment and molecular-level exploration of the mechanism of action of Nettle (*Urtica dioica* L.) plant extract as an eco-friendly corrosion inhibitor for X38 mild steel in sulfuric acidic medium. *Arabian Journal of Chemistry*, **16** (8). <https://doi.org/10.1016/j.arabjc.2023.104988>
- Feng, Y., He, J., Zhan, Y., An, J., Tan, B., 2021. Insight into the anti-corrosion mechanism Veratrum root extract as a green corrosion inhibitor. *Journal of Molecular Liquids* **334**, 116110. <https://doi.org/10.1016/j.molliq.2021.116110>
- Fidrusli, A., Suryanto, , Mahmood, M., 2018. Ginger extract as green corrosion inhibitor of mild steel in hydrochloric acid solution. *IOP Conference Series: Materials Science and Engineering* **290**, 012087. <https://doi.org/10.1088/1757-899x/290/1/012087>
- Wan, S., Zhang, T., Chen, H., Liao, B., Guo, X., 2022. Kapok leaves extract and synergistic iodide as novel effective corrosion inhibitors for Q235 carbon steel in H2SO4 medium. *Industrial Crops and Products* **178**, 114649. <https://doi.org/10.1016/j.indcrop.2022.114649>
- Chen, S., Zhu, B., Liang, X., 2020. Corrosion inhibition performance of coconut leaf extract as a green corrosion inhibitor for X65 steel in hydrochloric acid solution. *International Journal of Electrochemical Science* **15**, 1-15. <https://doi.org/10.20964/2020.01.39>
- Wan, S., Wei, H., Quan, R., Luo, Z., Wang, H., Liao, B., Guo, X., 2022. Soybean extract firstly used as a green corrosion inhibitor with high efficacy and yield for carbon steel in acidic medium. *Industrial Crops and Products* **187**, 115354. <https://doi.org/10.1016/j.indcrop.2022.115354>
- Wang, D-Yang., Li, H-Jing., Chen, X., Nie, B-Li., Wu, Y-Chao., 2022. Fabricating of grape seed proanthocyanidins loaded Zein-NaCaS composite nanoparticles to exert effective inhibition of Q235 steel corrosion in seawater. *Journal of Molecular Liquids* **348**, 118467. <https://doi.org/10.1016/j.molliq.2022.118467>
- Wan, S., Chen, H., Zhang, T., Liao, B., Guo, X., 2021. Anti-corrosion mechanism of parsley extract and synergistic iodide as novel corrosion inhibitors for carbon steel-Q235 in acidic medium by electrochemical, XPS and DFT methods. *Frontiers in Bioengineering and Biotechnology* **9**, 815953. <https://doi.org/10.3389/fbioe.2021.815953>
- Li, X., Deng, S., Du, G., Xie, X., 2020. Synergistic inhibition effect of walnut green husk extract and sodium lignosulfonate on the corrosion of cold rolled steel in phosphoric acid solution. *Journal of Taiwan Institution of Chemical Engineers* **114**, 263-283. <https://doi.org/10.1016/j.jtice.2020.09.010>
- Arellanes-Lozada, P., Díaz-Jiménez, V., Hernández-Cocolezzi, H., Nava, N., Olivares-Xometel, O., Likhanova, N.V., 2020. Corrosion inhibition properties of iodide ionic liquids for API 5L X52 steel in acid medium. *Corrosion Science* **175**, 108888. <https://doi.org/10.1016/j.corsci.2020.108888>
- Kaya, F., Solmaz, R., Geçibesler, Ibrahim.H., 2023. Investigation of adsorption, corrosion inhibition, synergistic inhibition effect and stability studies of Rheum ribes leaf extract on mild steel in 1 M HCl solution. *Journal of Taiwan Institution of Chemical Engineers* **143**, 104712. <https://doi.org/10.1016/j.jtice.2023.104712>
- Bouhlal, F., Mazkour, A., Labjar, H., Benmessaoud, M., Serghini-Idrissi, M., El Mahi, M., Lotfi, E.M., El Hajjaji, S., Labjar, N., 2020. Combination effect of hydro-alcoholic extract of spent coffee grounds (HECG) and potassium Iodide (KI) on the C38 steel corrosion inhibition in 1M HCl medium: Experimental design by response surface methodology. *Chemical Data Collections* **29**, 100499. <https://doi.org/10.1016/j.cdc.2020.100499>
- Zhang, F., Xin, X., Ran, L., Li X., 2022. Inhibition Effect of Orange Peel Extract on Aluminum in Hydrochloric Acid Solution. *Journal of Southwest Forest University* **42**, 103-110. <https://doi.org/10.11929/j.swfu.202101009>
- Zhou, K., Liu, X., Liu, S., 2023. Corrosion inhibition of navel orange peel extract to stainless steel in acidic medium. *Journal of Chinese Society for Corrosion and Protection* **43**, 619-629. <https://doi.org/10.11902/1005.4537.2022.214>
- Liu, X., Guan, J., Fu, Z., Zhao H., Zhang Q., Li F., Wang L., Ma N., Li B., Wei H., 2023. Corrosive inhibiting ability and Mechanism of Orange Peel Extract in H3PO4 Solution. *SURF Technology* **52**, 263-277. <https://doi.org/10.16490/j.cnki.issn.1001-3660.2023.08.021>
- Raghu, A.V., Anita, G., Barigaddi, Y.M., Gadaginamath, G.S., Aminabhavi, T.M., 2007. Synthesis and characterization of novel polyurethanes based on 2,6-bis(4-hydroxybenzylidene) cyclohexanone hard segments. *Journal of Applied Polymer Science* **104**, 81-88. <https://doi.org/10.1002/app.25518>
- Li, X., Deng, S., Xie, X., Fu, H., 2014. Inhibition effect of bamboo leaves' extract on steel and zinc in citric acid solution. *Corrosion Science* **87**, 15-26. <https://doi.org/10.1016/j.corsci.2014.05.013>
- Luo, W., Lin, Q., Ran, X., Li, W., Tan, B., Fu, A., Zhang, S., 2021. A new pyridazine derivative synthesized as an efficient corrosion inhibitor for copper in sulfuric acid medium: Experimental and theoretical calculation studies. *Journal of Molecular Liquids* **341**, 117370. <https://doi.org/10.1016/j.molliq.2021.117370>
- Wang, X., Ren, S., Zhang, D., Jiang H., Gu, Y., 2019. Inhibition Effect of Soybean Meal Extract on Corrosion of Q235 Steel in Hydrochloric Acid Medium. *Journal of Chinese Society for Corrosion and protection* **39**, 267-273. <https://doi.org/10.11902/1005.4537.2018.118>
- Tang, M., Li, X., Deng, S., Lei, R., 2021. Synergistic inhibition effect of Mikania micrantha extract with KI on steel corrosion in H2SO4 solution. *Journal of Molecular Liquids* **344**, 117926. <https://doi.org/10.1016/j.molliq.2021.117926>
- Teng, X., Deng, S., Li, X., 2024. Synergistic corrosion inhibition of rubber seed extract with KI on cold rolled steel in sulfuric acid solution. *Journal of Taiwan Institution of Chemical Engineers* **161**, 105564. <https://doi.org/10.1016/j.jtice.2024.105564>
- Du, P., Deng, S., Du, G., Shao, D., Xu, D., Li, X., 2023. Synergistic inhibition effect of Mikania micrantha extract with potassium iodide on the corrosion of cold rolled steel in methanesulfonic acid solution. *Corrosion Science* **220**, 111296. <https://doi.org/10.1016/j.corsci.2023.111296>
- Zhao, H., Deng, S., Qiang, Y., Xu, J., Xu, D., Li, X., 2024. Synergistic mixture of Camellia Oleifera shell extract and KI as an eco-friendly and highly efficient composite inhibitor for steel corrosion in H2SO4 media. *Journal of Molecular Liquids* **407**, 125164. <https://doi.org/10.1016/j.molliq.2024.125164>
- Wang, Q., Wang, R., Zhou, X., Aslam, R., Sun, X., Zhang, Q., Zhao, C., Sun, Y., Yan, Z., Li, X., 2024. Investigating the synergistic effect of iodide ion and Michelia alba leaf extract on carbon steel in 0.5 M H2SO4. *Materials Today Communications* **40**, 109696. <https://doi.org/10.1016/j.mtcomm.2024.109696>
- Zhang, S., Liu, S., Zhu, Z., Hu, Y., 2017. Extraction of active components from pomelo peel and study on their corrosion inhibiting ability. *Fine & Speciality Chemicals* **25**, 27-32. <https://doi.org/10.19482/j.cn11-3237.2017.01.05>
- Hosseini, M., Mertens, S.F.L., Arshadi, M.R., 2003. Synergism and antagonism in mild steel corrosion inhibition by sodium dodecylbenzenesulphonate and hexamethylenetetramine. *Corrosion Science* **45**, 1473-1489. [https://doi.org/10.1016/s0010-938x\(02\)00246-9](https://doi.org/10.1016/s0010-938x(02)00246-9)
- Gao, H., Xie, N., Wang, H., Chen, M., Zhang, J., Sun, J., Jin, Z., 2020. Evaluation of corrosion inhibition performance of a novel ionic liquid based on synergism between cation and anion. *New Journal of Chemistry* **44**, 7802-7810.
- Zhu, H., Li, X., Lu, X., Chen, X., Li, J., Han, X., Ma, X., Hu, Z., 2021. Intra-/inter-molecular synergistic inhibition effect of sulfonate surfactant and 2-benzothiazolethiol on carbon steel corrosion in 3.5% NaCl solution. *Corrosion Science* **182**, 109291. <https://doi.org/10.1016/j.corsci.2021.109291>
- Behpour, M., Ghoreishi, S.M., Khayatkhani, M., Soltani, N., 2012. Green approach to corrosion inhibition of mild steel in two acidic solutions by the extract of Punica granatum peel and main constituents. *Materials Chemistry and Physics* **131**, 621-633. <https://doi.org/10.1016/j.matchemphys.2011.10.027>
- Jessima, S.J.H.M., Subhashini, S., Arulraj, J., 2020. Sunova spirulina powder as an effective environmentally friendly corrosion inhibitor for mild steel in acid medium. *Journal of Bio- and Tribo-Corrosion* **6**. <https://doi.org/10.1007/s40735-020-00370-x>
- Mobin, M., Rizvi, M., 2017. Adsorption and corrosion inhibition behavior of hydroxyethyl cellulose and synergistic surfactants additives for carbon steel in 1 M HCl. *Carbohydrate Polymer* **156**, 202-214. <https://doi.org/10.1016/j.carbpol.2016.08.066>
- Li, X., Deng, S., Lin, T., Xie, X., 2019. Cassava starch graft copolymer as a novel inhibitor for the corrosion of aluminum in HNO3 solution. *Journal of Molecular Liquids* **282**, 499-514. <https://doi.org/10.1016/j.molliq.2019.03.044>
- Ahmed, S.K., Ali, W.B., Khadam, A.A., 2019. Synthesis and investigations of heterocyclic compounds as corrosion inhibitors for mild steel in hydrochloric acid. *International Journal of Industrial Chemistry* **10**, 159-173. <https://doi.org/10.1007/s40090-019-0181-8>
- Zakaria, K., Hamdy, A., Abbas, M.A., Abo-Elenien, O.M., 2016. New organic compounds based on siloxane moiety as corrosion inhibitors for carbon steel in HCl solution: Weight loss, electrochemical and surface studies. *Journal of Taiwan Institution of Chemical Engineers* **65**, 530-543. <https://doi.org/10.1016/j.jtice.2016.05.036>
- Zarrok, H., Zarrouk, A., Hammouti, B., Salghi, R., Jama, C., Bentiss, F., 2012. Corrosion control of carbon steel in phosphoric acid by purpald – weight loss, electrochemical and XPS studies. *Corrosion Science* **64**, 243-252. <https://doi.org/10.1016/j.corsci.2012.07.018>
- He, X., Jiang, Y., Li, C., Wang, W., Hou, B., Wu, L., 2014. Inhibition properties and adsorption behavior of imidazole and 2-phenyl-2-imidazoline on AA5052 in 1.0M HCl solution. *Corrosion Science* **83**, 124-136. <https://doi.org/10.1016/j.corsci.2014.02.004>
- Akin, M., Saki, N., 2018. Monopropylene glycol based heat transfer fluid: effects of green and synthetic corrosion inhibitors on copper and aluminum with ageing tests. *Anti-Corrosion Methods and Materials* **65**, 11-18. <https://doi.org/10.1108/acmm-02-2017-1766>

45. Salmasifar, A., Edraki, M., Alibakhshi, E., Ramezanzadeh, B., Bahlakeh, G., 2021. Combined electrochemical/surface investigations and computer modeling of the aquatic Artichoke extract molecules corrosion inhibition properties on the mild steel surface immersed in the acidic medium. *Journal of Molecular Liquids* **327**, 114856. <https://doi.org/10.1016/j.molliq.2020.114856>
46. Zhang, Q.H., Hou, B.S., Li, Y.Y., Zhu, G.Y., Liu, H.F., Zhang, G.A., 2020. Two novel chitosan derivatives as high efficient eco-friendly inhibitors for the corrosion of mild steel in acidic solution. *Corrosion Science* **164**, 108346. <https://doi.org/10.1016/j.corsci.2019.108346>
47. Qu, Q., Jiang, S., Li, L., Bai, W., Zhou, J., 2008. Corrosion behavior of cold rolled steel in peracetic acid solutions. *Corrosion Science* **50**, 35-40. <https://doi.org/10.1016/j.corsci.2007.06.008>
48. Haque, J., Srivastava, V., Chauhan, D.S., Lgaz, H., Quraishi, M.A., 2018. Microwave-induced synthesis of chitosan schiff bases and their application as novel and green corrosion inhibitors: Experimental and theoretical approach. *ACS Omega* **3**, 5654-5668. <https://doi.org/10.1021/acsomega.8b00455>
49. Saxena, A., Prasad, D., Thakur, K.K., Kaur, J., 2021. PDP, EIS, and surface studies of the low-carbon steel by the extract of *Tinospora cordifolia*: A green approach to the corrosion inhibition. *Arabian Journal for Science and Engineering* **46**, 425-436. <https://doi.org/10.1007/s13369-020-04894-9>
50. Chung, I-Min., Malathy, R., Priyadharshini, R., Hemapriya, V., Kim, S-Hyun., Prabakaran, M., 2020. Inhibition of mild steel corrosion using *Magnolia kobus* extract in sulphuric acid medium. *Materials Today Communications* **25**, 101687. <https://doi.org/10.1016/j.mtcomm.2020.101687>
51. Li, X., Deng, S., 2020. Synergistic inhibition effect of walnut green husk extract and potassium iodide on the corrosion of cold rolled steel in trichloroacetic acid solution. *Journal of Materials Research and Technology* **9**, 15604-15620. <https://doi.org/10.1016/j.jmrt.2020.11.018>
52. Wang, Q., Zhang, Q., Zheng, H., Liu, L., Wu, X., Zhao, C., Zhou, X., Sun, Y., Yan, Z., Li, X., 2023. Insight into anti-corrosion behavior of protein extract as eco-friendly corrosion inhibitor. *Sustainable Chemistry and Pharmacy* **34**, 101177. <https://doi.org/10.1016/j.scp.2023.101177>
53. Elmeligi, A., Ismail, N., 2009. Hydrogen evolution reaction of low carbon steel electrode in hydrochloric acid as a source for hydrogen production. *International Journal of Hydrogen Energy* **34**, 91-97. <https://doi.org/10.1016/j.ijhydne.2008.10.026>